Investigation of optical properties of aging soot

Migliorini, F.; Thomson, K. A.; Smallwood, G. J.

Publisher's version / Version de l'éditeur:
https://doi.org/10.1007/s00340-011-4396-4
Applied Physics B, 104, 2, pp. 273-283, 2011-02-12

Appl Phys B
DOI 10.1007/s00340-011-4396-4

Applied Physics B
Lasers and Optics

Investigation of optical properties of aging soot

F. Migliorini · K.A. Thomson · G.J. Smallwood

Received: 18 October 2010 / Revised version: 14 December 2010

Abstract The optical properties of soot, in particular the propensity of soot to absorb and scatter light as a function of wavelength, are key parameters for the correct interpretation of soot optical diagnostics. An overview of the data available in the literature highlights the differences in the reported optical properties of aging soot. In many cases, the properties of mature soot are used when evaluating in-flame soot but this assumption might not be suitable for all conditions and should be checked. This need has been demonstrated by performed spectral resolved line-of-sight attenuation (Spec-LOSA) measurements on an ethylene/air premixed and non-premixed flame. Transmission electron microscopy of thermophoretically sampled soot was also performed to qualify the soot aging and to establish soot morphology in order to correct light extinction coefficients for the scattering contribution. The measured refractive index absorption function, $E(m)_\lambda$, showed a very strong spectral dependence which also varied with height above the burner for both flames. However, above 700 nm, the slope of the refractive index function was near zero for both flames and all measurement heights. The upper visible and near infrared wavelengths are therefore recommended for soot optical measurements.

F. Migliorini · K.A. Thomson (✉) · G.J. Smallwood
Institute for Chemical Process and Environmental Technology, National Research Council of Canada, 1200 Montreal Road, Ottawa, Ontario K1A 0R6, Canada
e-mail: Kevin.Thomson@nrc-cnrc.gc.ca
Fax: +1-613-9577869

F. Migliorini
e-mail: Francesca.Migliorini@nrc-cnrc.gc.ca

G.J. Smallwood
e-mail: Greg.Smallwood@nrc-cnrc.gc.ca

1 Introduction

Recent research and development in the area of combustion have been motivated by the commitment of preserving a clean environment and to reduce the health impact of airborne species such as soot particles and polycyclic aromatic hydrocarbons. Soot formation also plays an important role in the performance of all combustion processes. Therefore, it is mandatory to have accurate measurement techniques for in-situ characterization of soot during its formation, and to quantify soot emissions. The former is critical for the validation of combustion models and soot formation submodels, while the latter is needed to assess emission factors for complex combustion systems and to evaluate emission reduction strategies. Many optical diagnostic techniques have been developed for these purposes over the last several decades. These methods can offer remote, nonintrusive, in situ, spatially and temporally precise measurements of important parameters including soot concentration and morphology and so they are particularly suitable for the combustion environment. In particular, the two-color method has been widely used in diesel engines in order to measure flame temperature and KL factor, which is proportional to the soot concentration. The light extinction technique has also been a popular and accurate way to measure soot concentration, and combined with light scattering can be used to measure soot particle size. The Laser-Induced Incandescence (LII) technique has emerged as an attractive method for real-time soot concentration monitoring in practical devices [1]. This technique has been extensively used to measure soot particulate emissions from diesel and gasoline engines and from gas turbines, soot concentrations in laboratory flames, and black carbon in the ambient environment. Nevertheless, the interpretation of soot optical diagnostics requires the knowledge of the optical properties of soot; specifically, the propensity of soot to absorb and scatter light as a function of its

Published online: 12 February 2011

wavelength. This property is also exploited by most of the commercially available instruments developed to evaluate the emission of light absorbing particles. These instruments implement filter-based (absorption or reflectance), photoacoustic, refractive-index-based, extinction-scattering, or LII techniques [2] and, therefore, the measured particulate concentrations are affected by the soot optical properties used for the evaluation. Moreover, soot optical properties are of particular importance in the interpretation of soot pyrometry, where emission at two or more wavelengths is used to determine soot temperature and concentration [3–6]. Many studies of soot optical properties are presented in the literature [7–19], but they show large uncertainties and discrepancies and are predominantly focused on mature post-flame soot.

The question arises as to whether these optical properties are the appropriate ones to use when performing in-flame measurements, where soot varies from incipient to mature through solidification, surface growth, aggregation, oxidation, and cooling. In-flame soot aging has been observed from TEM studies where young soot appears liquid-like on TEM grids and has poor contrast [20–22] whereas mature soot exhibits good contrast in TEM images and has distinct aggregated structures of primary particles. It is reasonable to assume that optical properties of the soot change concurrently. Indeed, some evidence of a changing spectral dependence or soot aging in a premixed flame at low pressure has also been observed by Cléon et al. [23]. They determine the ratio of $E(m_\lambda)$ at 532 nm and 1064 nm by a two excitation color laser induced incandescence method [24]. They find that the ratio varies as function of the height above the burner (HAB) with a ratio of 1.97 at 12 mm HAB but monotonically decreasing to a plateau value of 1.37 for heights greater than 28 mm HAB. This finding suggests a variation of the soot optical properties with age with the eventual stabilization to some mature soot, though it is noted that the stable ratio achieved was not the value of 1 often supposed for mature soot. Bladh et al. have also studied the variation of the absolute magnitude of $E(m_\lambda)$ of in-situ soot as a function of height in an atmospheric pressure McKenna burner, following a methodology developed by Snelling and Liu [25] and found an increasing $E(m_\lambda)$ with increasing HAB before stabilizing to a constant value [26].

Beyond the possibility of changing optical properties of soot, other species such as large PAH molecules are known to absorb and emit light in the ultraviolet (UV) and visible wavelengths, and thus could interfere with soot measurements. While some groups have attributed measurements at 532 nm to soot exclusively [27], others find that higher wavelengths are necessary to avoid potential interferences from nonsoot species [28, 29].

Despite these recommendations, many contemporary in-flame studies of soot use visible wavelengths for soot detection and the optical properties of mature, post-flame soot in the measurement evaluation (e.g., [30–45]). The same is true of commonly used commercial soot detection systems [2]. We hypothesize that the assumption of invariant optical properties is not valid and can lead to substantial error in the interpretation of in-flame measurements.

Non-premixed combustion is typical of practical combustion system and, therefore, in spite of the complex flame geometry, coflowing non-premixed flames have been widely investigated by means of optical diagnostics in order to study soot formation and growth processes [46, 47]. The McKenna burner [48] is another example of a burner widely used in the literature. The flame is considered as a standard in lean and close-to-stoichiometric conditions and employed in many laboratories around the world for the development and calibration of optical diagnostic techniques [49–52]. The flame is designed and assumed to be one-dimensional, which allows simplified combustion modeling. Therefore, several studies performed under rich conditions have studied the mechanism of soot formation, combining optical and sampling techniques with detailed chemical kinetics simulations [43, 53–56]. Moreover, this burner is used as a standard for the development of the laser-induced incandescence (LII) technique [34, 57, 58].

In the present work, we investigate a rich ethylene/air premixed flame produced by a McKenna burner in a standard condition adopted for intercomparison by the LII community and a Gülder laminar ethylene/air co-annular non-premixed flame. Spectrally resolved line-of-sight attenuation (Spec-LOSA) measurements have been performed to quantify the spectral variation of the refractive index absorption function at various heights in two typical laboratory flames and to determine if there is a wavelength threshold above which optical properties can be considered stable. Attenuation measurements are corrected for light scattering contribution using soot morphology determined from Transmission Electron Microscopy (TEM). We show that the measured refractive index absorption function, $E(m)_\lambda$, which potentially includes effects of nonsoot light absorbing constituents, has a very strong spectral dependence which varies with height above the burner. The implications of the measurements are discussed in terms of their impact on flame emission and in-situ laser-induced incandescence measurements.

2 Soot optical properties in the literature

The optical properties of soot have been studied for many years with particular attention focused on refractive index. However, the spread of the soot refractive indices reported in the literature is quite wide even when restricted to the visible wavelengths [7–9, 13, 16]. Various arguments have been stated with regard to which optical property measurements are valid and which ones should be excluded [59] but

ultimately large uncertainties remain. Through this debate, a key observation sometimes made but often not emphasized is that various types of carbon particles are produced during combustion processes and that these different particles have different optical properties which may also change as the particles age from young soot to mature soot. In a recent paper, Andreae et al. [60] reported definitions of various types of atmospheric carbon, such as soot carbon, brown carbon, light absorbing carbon, elemental carbon, and black carbon. These classes of absorbers are not universally recognized and the distinction between them is not clear. Nevertheless, as an example, a different spectral dependence of light absorption by black carbon and brown carbon has been found [2, 59, 60] where the refractive index of soot carbon is often observed to be wavelength independent, while brown carbon has an enhanced absorption in the UV. This might be related to differences in the elemental composition, typically in the H/C ratio, even if some conflicting results on the relationship between H/C ratio and refractive index have been presented [7, 61]. According to Alfé et al. [62], the nature of the fuel and soot aging are responsible for variations in the internal nanostructure of soot, resulting in diverse spectral features. The variations in the internal structure of soot primary particles results from different soot inception mechanisms occurring in flames that are more or less rich in the aromatic species considered to be soot precursors. Other important parameters to take into account when considering in-flame soot are the residence time and burner type [63]. Varying the flame geometry, it is possible to influence the heating of the fuel stream and consequently the soot formation and growth processes. As a consequence, the concentration of soot precursor particles and polycyclic aromatic hydrocarbons (PAHs), which are sufficiently large to absorb and emit light in the upper UV and lower visible wavelengths, can be enhanced to the point where they influence soot optical diagnostics.

Finally, it is noted that in the early 1990s, two groups of researchers reported the existence of 2–4 nm nonsoot nanoparticles in flames, with different properties and roles in soot formation [64]. According to D'Alessio et al. [53, 65] these particles, observed in rich premixed ethylene/oxygen flames, are strong absorbers in the UV but are transparent in the visible and can be thought of as polymer-like structures containing sub-structures with aliphatic aromatic (2–3 ring) bonds. Conversely, in observing the mass spectra of soot precursors in a nonsmoking ethylene non-premixed flame, Dobbins et al. [66] recognized similar particles as layers of fully condensed large PAHs and noted that they should be capable of absorbing in the visible. Several new methods for nanoparticle measurements have been developed recently as summarized in a review by D'Anna [27].

In contrast to the confusing and sometimes contradictory observations summarized from the literature above, some measurements and a literature review focused on post-flame soot have observed somewhat more consistent optical properties for soot [56, 67, 68] for fuels ranging from light gases to liquids. This suggests that given sufficient time or the opportunity to cool to ambient temperatures, soot may in fact stabilize to a form which exhibits reliable optical properties. While this may be true, it does not resolve the problem of selecting optical properties for the analysis and interpretation of in-flame soot measurements.

Much more has been stated on this complex and contentious topic than can be summarized here. However, we observe that attribution of soot optical properties to in-flame soot is not trivial, and consequently the validity of in-flame optical measurements of soot needs to be examined closely.

3 Theory

Line-of-sight-attenuation (LOSA) is a well-established soot diagnostic valuable for soot volume fraction, f_v, mapping [33, 36, 69, 70]. In LOSA measurements, the optical transmissivity of an aerosol containing medium is measured along a linear path through the medium. The transmissivity of the path, τ_λ, at wavelength λ, is measured as the ratio of light intensity before, $I_{\lambda,0}$, to that after passing through the attenuating medium, I_λ. The transmissivity is functionally related to a line integral of the local extinction coefficients, K^e_λ, along the path via:

$$\tau_\lambda = \frac{I_\lambda}{I_{\lambda,0}} = \exp\left(-\int_{-\infty}^{\infty} K^e_\lambda \, \mathrm{d}s\right) \tag{1}$$

where s is the spatial location along the path. In media where the soot concentration is not uniform along the measurements chord, a single transmissivity measurement can only provide a measure of the average soot concentration. However, in system with axial symmetrical geometry, a tomographic inversion algorithm [57] can be applied to achieve local values of the extinction coefficient and consequently radially resolved soot concentration. On the other hand, if the medium is uniform along the line-of-sight, (1) simplifies to:

$$-\ln \tau_\lambda(y) = K^e_\lambda L \tag{2}$$

where L is the length of the chord through the medium. For a horizontal chord through the centerline of a McKenna burner this simplification is approximately true.

According to RDG-FA (Rayleigh–Debye–Gans–Fractal Aggregate) theory for fractal aggregates made up of primary particles that fall in the Rayleigh range [71] (i.e., $\pi d_p/\lambda < 0.3$, where d_p is the diameter of a primary par-

ticle), soot concentration is related to the extinction, absorption and scattering coefficients as

$$f_v = \frac{K_\lambda^a \lambda}{6\pi E(m_\lambda)} = \frac{K_\lambda^e \lambda}{6\pi(1+\rho_{sa,\lambda})E(m_\lambda)} \tag{3}$$

where $E(m_\lambda)$ is the soot absorption function, $\rho_{sa,\lambda}$ is the ratio of the total scatter cross-section (over $4*\pi$ steradian), σ_λ^s, to the absorption coefficient, σ_λ^a [71–73]. The total scatter cross-sections can be estimated via RDG-FA theory, integrating the differential scattering cross-section of the aggregates over the aggregate size distribution and over 4π steradians. A detailed summary of the method can be found in [74] and follows the approach of Sorensen [73]. The calculation requires knowledge of the soot morphology (e.g., the primary particle diameter and number of particles per aggregate). For the present work, morphology was determined by thermophoretic sampling and TEM imaging as described in the apparatus section.

In circumstances where light scatter is negligible (i.e., for very small soot aggregates) or for soot of known morphology, Spec-LOSA provides a valuable tool to investigate the relative variation of $E(m_\lambda)$ with λ:

$$E(m_\lambda) = \frac{K_\lambda^a \lambda}{6\pi f_v} \propto K_\lambda^a \lambda = \frac{K_\lambda^e \lambda}{1+\rho_{sa,\lambda}} \tag{4}$$

since f_v is constant in a given measurement. Absolute measurement of $E(m_\lambda)$ is possible if f_v can be unequivocally measured by another method such as gravimetric sampling (e.g., [74]). If is noted that in the above analysis, it is implicitly assumed that soot is the only constituent in the optical path absorbing light. In fact, and as discussed above, large PAH and nonsoot nanoparticles may also contribute and so the measured refractive index function is effective in that it includes influence of these other species. The implication of such interferences is discussed in the discussion section.

4 Apparatus

In this work, both a premixed flat flame and a laminar non-premixed flame were investigated. The ethylene/air premixed flame was produced on a bronze porous plug McKenna burner (inner-plug diameter 60 mm) at atmospheric pressure. The total fuel/air flow rate was 10 l/min and the equivalence ratio was 2.1. To shield the flame from the surrounding air, an external shroud of nitrogen, flowing at 15 l/min, was used. Moreover, for flame stabilization, a stainless steel plate of 60 mm diameter was placed at 21 mm above the burner. All the flows were regulated by Brooks mass flow controllers calibrated at 20°C and atmospheric pressure. The ethylene/air non-premixed flame was produced by a Gülder laminar coannular burner [75]. Fuel is emitted from a central steel fuel nozzle with an outside diameter (o.d.) of 12.7 mm and an inside diameter (i.d.) of 10.9 mm. Air is emitted from a co-annular tube with an i.d. of 88 mm. The air flow is straightened using a combination of glass beads and sintered metal foam. The air flow rate was 284 lpm (20°C, atmospheric pressure) and the fuel at 0.194 lpm. In both cases, the measurements were performed at several heights above the burner (HAB) in order to follow the soot inception, growth, and aging processes.

To gain information on soot morphology, thermophoretic sampling, and transmission electron microscopy (TEM) analysis were performed. Thermophoretic sampling was achieved using probe on which a carbon coated copper TEM grids (3 mm diameter) were attached. The probe insertion, exposure, and withdrawn were controlled by a double-acting pneumatic cylinder system, with which the sampling time duration was adjustable. In the case of the McKenna burner, the sampling time was set to 80 ms and the sampling location was at the centerline of the flame at a height of 12 mm above the burner. For the Gülder burner, a sampling exposure time of 25 ms was used and samples were collected at 10 mm in the annular region ($r = 3.5$ mm) and at 42, 50, and 55 mm at the centerline. Three grids were collected at each height and analyzed using a 120 kV transmission electron microscope (Philips CM20) at different magnification, high magnification for the primary particle diameter analysis, and an intermediate magnification for the aggregates analysis. The images were processed using commercial image processing software (Image-Pro Plus). The analysis of the primary particle diameters was made manually using particles whose borders could clearly be detected. The aggregates were automatically recognized by the software and a measurement tool was used in order to gain aggregates properties, such as the perimeter, the projected area, and the minimum and maximum caliper lengths.

The Spec-LOSA experimental apparatus used for the premixed flame is shown schematically in Fig. 1. An intense diffuse light produced by an Hg arc lamp was focused through a circular 1 mm diameter aperture, a_1, with a pair of optically conjugate achromatic lenses, L_1 (254 mm focal length, 50 mm diameter), with a nominal magnification of 1:1. The aperture plane was then imaged to the center of the flame with another pair of achromatic lens, L_2 (300 mm focal length, 50 mm diameter), again with the same magnification. In order to reduce depth-of-field blur of the beam over the 60 mm diameter of the flame, a rectangular aperture, a_2 (10 mm wide × 2 mm high), was placed between the two 300 mm focal length lenses. This achieves a high spatial resolution over the measurement depth-of-field in the vertical direction while allowing the beam to blur in the horizontal direction, which is appropriate for the one-dimensional McKenna burner flame. In order to provide a reference measurement of the lamp intensity before transmission through

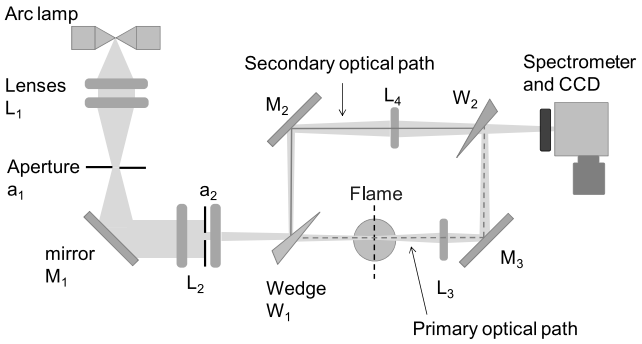

Fig. 1 Schematic of Spec-LOSA diagnostic for the premixed flame

the flame, the light beam was split into two paths by means of a wedge, W_1: the primary optical path passing through the center axis of the flame, while the secondary optical path bypasses the flame. The rectangular aperture was imaged using matched 200 mm focal length lenses, L_3 and L_4 (25.4 mm diameter), onto the vertical entrance slit of a spectrometer (nominal magnification 1:1), where the image location on the entrance slit was shifted vertically for one beam such that two signals, the lamp (our light source) and the transmission (both the lamp and the flame) were collected at the same time. In this way, any variation in lamp output during the acquisition period was captured.

The spectrometer (Jarell–Ash Monospec 18) was configured to measure in the wavelength range of 450 to 900 nm. This range was selected to optimize the combination of the output intensity of the lamp and the sensitivity of the detector, while avoiding second-order effects in the spectrometer since no band pass filters have been used. Measurement of the full spectral range with a single configuration of the system was critical due to problems with the repeatability of the McKenna burner. The CCD (Princeton Instrument–Spectrum MM System) attached to the output plane of the spectrometer records the two signals on one axis and wavelength on the orthogonal axis. The spectral resolution on the detector plane is 6.7 nm per pixel.

For the non-premixed flame the experimental set-up has been slightly modified. A tungsten strip lamp operating at 14 V, 7.3 A was used as light source since it has a smoother output spectrum which is ultimately better suited to spectral transmissivity measurements over a wider spectral range (450–1000 nm). However, measurement over this wavelength range required repositioning of the spectrometer grating (300 grooves/mm) and the use of band pass filters in order to avoid second-order effects. This was possible with the highly repeatable non-premixed flame. Each transmissivity curve is made by the combination of two data sets, the first capturing the range 450–800 nm and the second capturing 750–1150 nm. The lower range was filtered to eliminate light below 375 nm, while the upper range was filtered to eliminate light below 570 nm, which increased the sensitivity in that range while eliminating second-order effects.

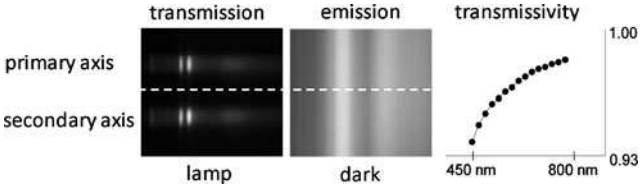

Fig. 2 Spec-LOSA measurements in ethylene/air premixed flame, 20 shot averages, HAB = 12 mm

Due to the shorter depth-of-field and the higher emission of the non-premixed flame, a larger rectangular aperture a_2 was used (10 mm wide × 4 mm high) in order to reduce the f number and increase the incident light.

A transmissivity measurement is typically achieved from two measurements. In the first measurement with the lamp unblocked, the spectra of both the lamp and attenuating medium (*transmission*) and the lamp without the attenuation medium present (*lamp*) are acquired via the primary and secondary optical axis. The lamp is then blocked and a second measurement is made of the flame alone (*emission*) and of the secondary axis in the absence of the lamp (*dark*). The transmissivity is defined as:

$$\tau_\lambda = \frac{transmission - emission}{lamp - dark} \tag{5}$$

At each measurement height, image sets consisted of 20 (premixed flame) or 30 (non-premixed flame) shot acquisitions for each measurement (*i.e.*, *transmission and lamp*, *emission* and *dark*). A typical set of images is shown in Figs. 2a and 2b where the horizontal axis of each image is the spectral axis. The upper spectrum in each image represents the intensity from the primary optical path (i.e. the light passing through the flame) and the lower spectrum is the secondary optical path. Whereas the raw data has a spectral resolution of 6.7 nm per pixel, the data used for calculations was binned into 49 nm bins (7 pixels) along the spectral axis and vertically over the height of each spectrum (100 pixels) to reduce shot noise. As noted above, 20 or 30 spectra were acquired for each measurement and, therefore, data averaging could also be used to improve the signal to noise ratio. Since the instantaneous lamp and transmission images were obtained synchronously and noting that the dark image has very little noise relative to the other images, the average transmissivity was calculated as

$$\overline{\tau_\lambda} = \frac{1}{n}\left[\sum_{i=1}^{n} \frac{transmission_l}{lamp_l - \overline{dark}} - \frac{\overline{emission}}{\overline{lamp} - \overline{dark}}\right] \tag{6}$$

In this way, *transmission* measurements are corrected for variation of the lamp intensity frame-by-frame. As *emission* is acquired asynchronously to *lamp* these values are averaged before taking the ratio. Since the two optical paths do not necessarily have identical light transmission efficiencies,

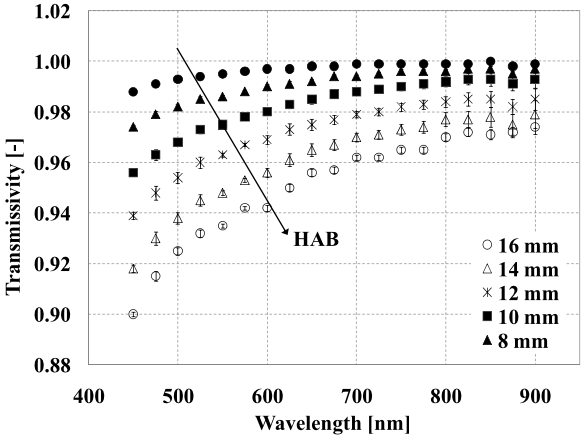

Fig. 3 Transmissivity at different heights above the burner in a premixed flame

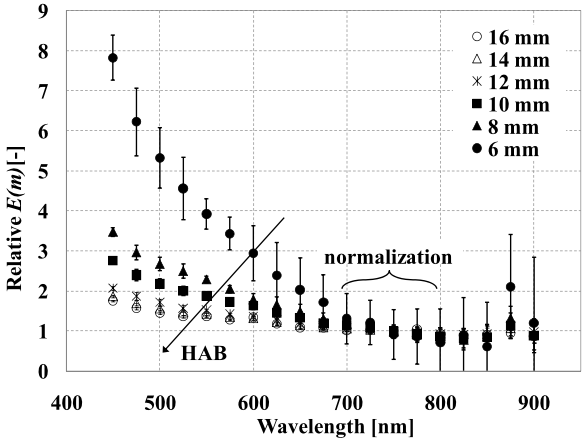

Fig. 4 Relative $E(m)_\lambda$ at different heights above the burner in a premixed flame

a normalization procedure was performed. A second set of spectra were taken in the absence of the flame, processed as the previous ones in order to obtain the normalization curve, $\tau_{\lambda,0}$. Finally, the normalized transmissivity was measured by the ratio $\tau_\lambda/\tau_{\lambda,0}$. Uncertainty of the transmissivity measurements were evaluated from the frame-to-frame variation of the multishot data acquisitions.

5 Results

5.1 Premixed flame

Since the McKenna burner is quasi one-dimensional, only single line-of-sight transmissivity measurements were performed on the centerline in order to get a line integrated extinction coefficient via (2). The spectral variation of the transmissivity at different heights above the burner is illustrated in Fig. 3 showing a strong increasing light attenuation with increasing height in the flame. For heights below 6 mm, extinction levels were too low to obtain a useful measure of the transmissivity. Above 16 mm, interference of the light beam by soot build up on the underside of the stabilization plate made measurements unreliable. The greatest attenuation occurs at the shortest wavelengths, where a strong contribution to absorption from PAHs and condensed species [76, 77] can be expected.

Thermophoretic sampling and transmission electron microscopy (TEM) analysis were performed in order to evaluate the scattering contribution. Soot morphology parameters were measured as $D_f = 1.65, k_f = 2.49, d_p = 20$ nm, $N_g = 9.91$, and $\sigma_g = 2.77$. A correction for scattering has been calculated following the method outlined in [74]. At this height above the burner, the maximum correction for scattering is 4% at 450 nm and drops to 1.6% at 800 nm. Therefore, even if the primary particle diameter and the aggregation are expected to increase slightly with the height above the burner, in the present case, the approximation of negligible scattering is quite accurate. As described in Sect. 3 and in light of the negligible contribution from scattering to the extinction measurement, it is appropriate to assume that the product of integrated extinction coefficients and measurement wavelength is proportional to the soot refractive index absorption function, $E(m_\lambda)$.

Figure 4 shows the relative $E(m_\lambda)$ behavior as a function of HAB, where the data at each height is normalized to average value of 1 at the upper wavelengths (700–800 nm). It is noted that the "bump" observed at 875 nm is an artifact probably due to second-order effects. The curves vary significantly with wavelength at all the heights above the burner. The slopes of the curves are greater lower down in the flame, with a peak eight-fold variation at HAB = 6 mm over the range 450 nm to 800 nm. However, even at the height of 16 mm, the variation is still 45%. Nevertheless, for the present measurements is noted that at all measured heights, the relative $E(m_\lambda)$ leveled to almost constant values at the upper visible region of the spectrum.

Figure 4 also shows the uncertainty bars (2σ) associated with the frame-by-frame variation. High in the flame the uncertainty bars are not visible since they are mainly covered by the symbols, while lower down in the flame the uncertainties start to be quite significant. That can be related to the lower signal to noise ratio associated with the very low attenuation at 6 mm, as it is show in Fig. 3.

5.2 Non-premixed flame

The same investigation has been extended to a laminar non-premixed flame. In this case, the soot concentration shows an axisymmetric geometry so it is not uniform along the measurements chord. Therefore, the technique provides only a path-average measurement of extinction coefficient and not the local value. Figure 5 shows the average transmissivity curves at different height above the burner, measured

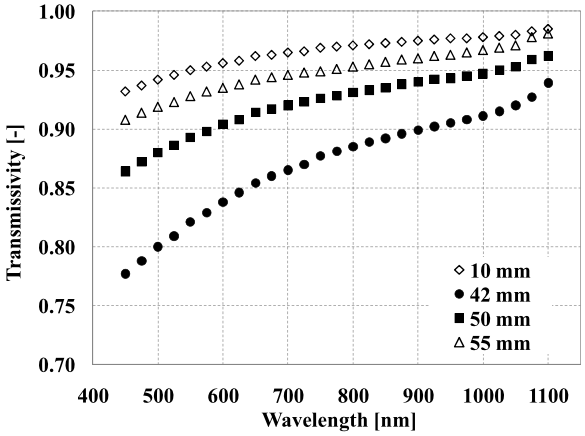

Fig. 5 Transmissivity at different heights above the burner in a non-premixed flame

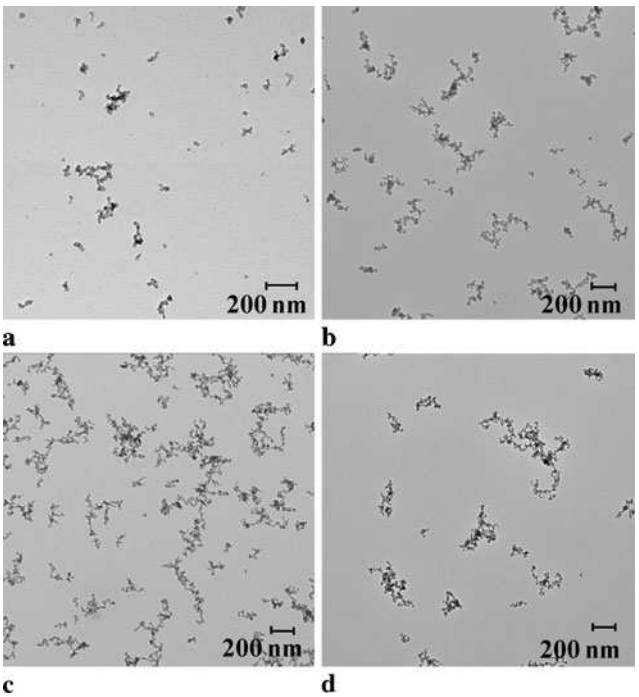

Fig. 6 Typical TEM images collected at 10 mm (**a**), 42 mm (**b**), 50 mm (**c**) and 55 mm (**d**) in a non-premixed flame

along the centerline at 42, 50, and 55 mm and through the external annulus region ($r = 3.5$ mm) at 10 mm, where the soot is localized according to the literature data [32].

It is well known from the literature [20] that soot aggregation in this kind of flame is quite significant, and this can lead to significant scattering relative to the absorption (i.e. $\rho_{sa,\lambda} \neq 0$). Therefore, soot morphology analysis was performed at all the four investigated heights. Thermophoretic sampling and TEM analysis were performed at the corresponding LOSA measurements location. Figure 6 shows typical sample from a TEM image at the different heights. At 10 mm, the aggregation is just beginning; few, quite small

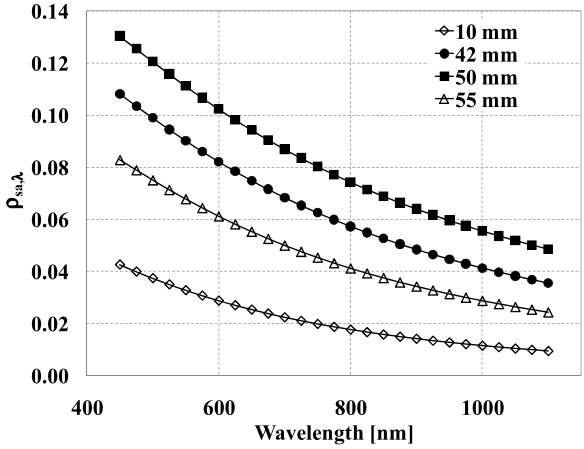

Fig. 7 Spectral scattering contribution to absorption at different heights above the burner in a non-premixed flame

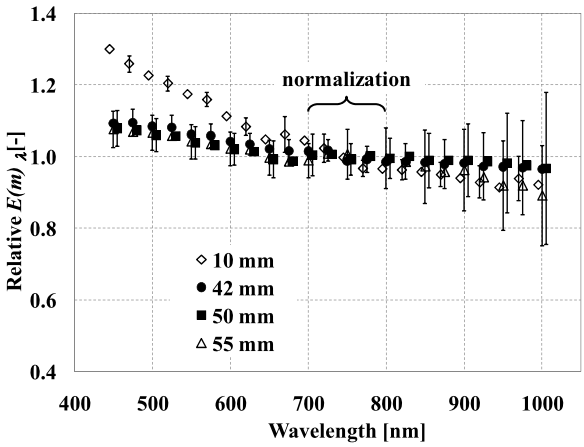

Fig. 8 Relative $E(m)_\lambda$ at different heights above the burner in a non-premixed flame

aggregates are observed together with some primary particles. Moreover, some, not well contrasted "dark spots" can be detected on the background, suggesting the presence of incipient soot particles or soot precursor at this height in the flame. Moving up through the flame the aggregation is definitively more pronounced and almost no primary particles are observed. The primary particles diameter increases with the height above the burner from 10 to 50 mm and then decreases at 55 mm where soot starts to oxidize. Following the same procedure as for the premixed flame, the scattering contribution to absorption has been calculated for the spectral range investigated. Figure 7 shows the $\rho_{sa,\lambda}$ curves at different heights above the burner. The scatter is almost negligible at 10 mm but becomes quite significant at 42 mm and 50 mm and it is still 8% at 55 mm for $\lambda = 450$ nm. As expected, scatter increases with decreasing wavelength. No formal uncertainty analysis has been performed on the $\rho_{sa,\lambda}$ data since the scattering to absorption ratio is dependent on many factors and form of the dependence is quite complex.

Nevertheless, as it is reported in the literature [78–80] the use of the RDG-PFA approximation introduce a 10% uncertainty in the aggregate absorption and total scattering cross sectional areas. Therefore, we assume that the $\rho_{sa,\lambda}$ values are no better than 10% uncertain.

In accordance with (3), the absorption coefficient is equal to the extinction coefficient scaled by $(1+\rho_{sa,\lambda})^{-1}$, so it is finally possible to have an estimation of the relative $E(m_\lambda)$ behavior since this quantity is directly proportional to $K_\lambda^a\lambda$. The relative $E(m_\lambda)$ behavior is reported in Fig. 8. Again a quite significant spectral variation is observed at all heights in the range 450–700 nm. The slope is greater at 10 mm, where prevalence of young, more hydrogenated soot is expected. At 42 and 50 mm, height soot should have reached its mature structure, while at 55 mm, which is close to the tip of the flame, it starts to oxidize. In fact, the three upper curves almost overlap in this range and this is in agreement with the assumption that mainly mature soot is present in this region of the flame. At higher wavelengths, around 700 nm, the curves start to level at 42 and 50 mm, while a slight decrease is observed at 10 and 55 mm in the range 700–1000 nm. At these two heights in the flame, the measurements are particularly sensitive to the flame stability, since in one case we were measuring at the edge on the flame and in the other we were really close to the tip. Nevertheless, within the uncertainties associated with these curves, relative $E(m_\lambda)$ is quite invariant with wavelength above 700 nm. In this case the uncertainty analysis takes into account both the uncertainties in $K_\lambda^e\lambda$ and $\rho_{sa,\lambda}$.

6 Discussion

The specific source of the variation of relative $E(m)_\lambda$ with height above burner for both flames is uncertain. Attenuation may come from large PAH molecules, semitransparent soot precursor nanoparticles, brown carbon, or black carbon. Each would have different spectral absorption tendencies and the overall relative $E(m)_\lambda$ variation could simply track the dominance of each class of absorber in the overall mixture as a function of height. Equally, particles in each class of absorbing species could be evolving such that their spectral characteristics change with height. Nevertheless, the nearly constant relative $E(m_\lambda)$ above 700 nm observed for both flames supports the assumption that attenuation or emission measurements are not affected by PAHs, condensed species or other non-soot particles in the upper visible or near infrared region of the spectrum. Whether the detected attenuation comes from soot or nonsoot species, the observed spectral variation of the relative $E(m_\lambda)$ and the difference of the result at different locations in the flame have significant implications for all soot optical diagnostics. In attenuation measurements, the measured soot volume fraction is inversely proportional to $E(m_\lambda)$ and all attenuation is attributed to soot. To avoid participation of large PAH in measurements, typically measurement wavelengths greater than 532 nm are recommended [16, 29, 58]. The present work suggests that 700 nm is the lower wavelength appropriate for this kind of absorption and emission measurements. This also confirms the observation of Zerb et al. [29] that even the HeNe laser operating at 632 nm is an insufficiently high wavelength for interference free measurement. In flame emission measurements, the influence is even more dramatic. For example, a two-color pyrometry measurement of soot emission at 450 and 800 nm in the McKenna burner at a height of 6 mm would overpredict the soot temperature by 450 K (for an initial temperature of 1800 K) and would underpredict the soot volume fraction by 88% if a constant $E(m_\lambda)$ was used when analyzing the data. At the standard height of 12 mm used in the LII community, the temperature would be overpredicted by 200 K and the soot volume fraction would be under-predicted by 63%. The implication of a varying relative $E(m_\lambda)$ for two-color LII measurements is less clear. While large PAHs and nanoparticles could contribute to attenuation and emission signals, it is less likely that they could be laser-heated to the same peak temperatures as soot without evaporating or sublimating and, therefore, their contribution to the total LII emission signal is uncertain. Conversely, if the soot is comprised of brown carbon (i.e., immature or high hydrogen content soot), attribution of an appropriate $E(m_\lambda)$ to the soot during LII signal analysis would be difficult and errors would propagate in a similar fashion to two color flame emission measurements. In addition, the findings have implications for the original one-wavelength version of the LII technique, in terms of quantitative measurements. For single wavelength LII, a calibration procedure is required in order to evaluate soot concentration from the LII signal. Most often this has been carried out employing a different technique, in general extinction. The accuracy of this technique is strongly dependent on the absolute value of $E(m_\lambda)$. The measurements are usually performed using a light source operating at 532 or 514 nm [34, 40, 41]. However, as discussed above, light absorption at these wavelengths can also come from various species other than soot which may or may not contribute to the LII emission.

The constancy of the relative $E(m_\lambda)$ above 700 nm also supports an invariance of the soot optical properties in the upper visible or near infrared region: however, this cannot be proven since the technique does not monitor the absolute magnitude of $E(m_\lambda)$ and this may be varying. Indeed, a recent paper by Bladh et al. [26] shows an increase in the magnitude of $E(m_\lambda)$ with increasing height in a similar flame. On the other hand, the finding of Bladh et al. involved LII measurement carried out at wavelengths of 445 and 575 nm and as discussed above the optical properties of soot at these wavelengths are quite uncertain.

7 Conclusions

It is evident from the current measurements that there is a great deal of uncertainty surrounding the correct soot refractive index absorption function to use when interpreting light absorption and emission measurements from soot and other absorbing/emitting species in a laminar premixed and non-premixed flame. While participation of large PAHs, condensed species and nanoparticles are likely contributors to the observed strong and height varying spectral behavior of relative $E(m)_\lambda$, it is not clear how they participate in emission and LII measurements. This behavior is critical to the correct interpretation of soot emission measurements and makes measurements essentially impossible without a priori knowledge of the relative $E(m_\lambda)$ function at the measurement location.

The results do show that the relative $E(m)_\lambda$ appears to stabilize above 700 nm in both premixed and non-premixed flames. Therefore, it is highly recommended to work above this wavelength to prevent absorption from nonsoot species thereby reduce the uncertainty in measurements induced by uncertainty in $E(m)_\lambda$. In spite of the fact that similar recommendations can be found in the literature, in many cases visible wavelengths are still used for absorption and emission measurements. Moreover, also most of the commercially available instruments developed for evaluated particulate emission use wavelengths in the visible region. Therefore, it is worthwhile to reemphasize the importance of using wavelengths in the upper visible and IR region of the spectra in the light of the present results. Unfortunately, it is not possible to ascertain from the measurements whether the absolute magnitude of $E(m_\lambda)$ is varying with height in the flame, though the constant slope of the relative $E(m_\lambda)$ above 700 nm suggests some stability to the soot optical property in this wavelength range.

Since the results indicate that as soot ages in the flame the optical properties change, care should be taken when calculations depend upon soot optical properties, as literature data for these properties may have been acquired under significantly different conditions than the intended application, and are likely to lead to significant errors. For the same reason, when using instruments dependent upon aspects of optical measurements, researchers should be aware that the calibration of the instrument may vary as the soot being measured varies in properties.

Future research will include LII measurements collected in the same flame with the objective of clarifying the contribution of nonsoot species to the absorption and to LII measurements, and to improve LII measurement interpretation.

Acknowledgement The authors would like to acknowledge financial support from a Helmholtz-DLR/NRC-ICPET collaboration.

Appendix

The relative soot absorption refractive function, $E(m_\lambda)_{\mathrm{rel}}$, obtained from (4), is recast in (A.1):

$$E(m_\lambda)_{\mathrm{rel}} = \frac{-\ln(\tau_\lambda)\lambda}{1+\rho_{sa,\lambda}}, \tag{A.1}$$

where $-\ln\tau_\lambda$ is used in place of K_λ^e. Error propagation analysis has been applied to (A.1) in order to estimate the uncertainty on $E(m_\lambda)_{\mathrm{rel}}$:

$$\frac{\sigma_E(m_\lambda)_{\mathrm{rel}}}{E(m_\lambda)_{\mathrm{rel}}} = \sqrt{\left(\frac{\sigma_{\tau\lambda}}{\ln(\tau_\lambda)\tau_\lambda}\right) + \left(\frac{\sigma_{\rho_{sa,\lambda}}}{1+\rho_{sa,\lambda}}\right)^2 + \left(\frac{\sigma_\lambda}{\lambda}\right)^2} \tag{A.2}$$

The first term is the contribution of uncertainty of the measured transmissivity and the second is the contribution of uncertainty in the ratio of total scatter to absorption. The final term is the contribution of uncertainty in the measurement wavelength which is included here for completeness but found to be negligible. As already mentioned, the uncertainty of $\rho_{sa,\lambda}$ has not been evaluated in this work. Rather, a 20% uncertainty (2σ) has been assumed in accordance with the literature [61].

As described in Sect. 4 the transmissivity is achieved by measuring the *transmission*, the *emission*, the *lamp* and the *dark*. Additionally, it was observed that a reference measurement is required where the flame is extinguished. The complete calculation of the normalized transmissivity is therefore:

$$\overline{\tau_{\lambda,\mathrm{nor}}} = \frac{\overline{\tau_\lambda}}{\overline{\tau_{\lambda,0}}} = \frac{\frac{1}{n}\left[\sum_{i=1}^{n}\frac{transmission_i}{lamp_i-\overline{dark}} - \frac{\overline{emission}}{\overline{lamp}-\overline{dark}}\right]}{\frac{1}{n}\left[\sum_{i=1}^{n}\frac{transmission_{i,0}}{lamp_{i,0}-\overline{dark_0}} - \frac{\overline{emission_0}}{\overline{lamp_0}-\overline{dark_0}}\right]} \tag{A.3}$$

The uncertainty of *dark* and $dark_0$ are found to be negligible and are not considered in the remainder of the analysis. Since *transmission* is collected synchronously with *lamp* and $transmission_0$ with $lamp_0$, it is appropriate to calculate the first terms in the numerator and denominator and assigning an uncertainty based on the n determinations. Conversely, emission is collected asynchronously to lamp and so the averages are used in the ratio and uncertainty is assessed based on the fluctuations of the measured terms. To facilitate the presentation of the uncertainty analysis, (A.3) is simplified to

$$\tau_{\lambda,\mathrm{nor}} = \frac{a-\frac{b}{c}}{a_0-\frac{b_0}{c_0}} \tag{A.4}$$

from which uncertainty is assessed from error propagation analysis:

$$\sigma_{\tau_{\lambda,\mathrm{nor}}} = \sqrt{\left(\frac{\partial \tau_{\lambda,\mathrm{nor}}}{\partial a}\sigma_a\right)^2 + \left(\frac{\partial \tau_{\lambda,\mathrm{nor}}}{\partial b}\sigma_b\right)^2 + \left(\frac{\partial \tau_{\lambda,\mathrm{nor}}}{\partial b}\sigma_b\right)^2 + \left(\frac{\partial \tau_{\lambda,\mathrm{nor}}}{\partial a_0}\sigma_{a_0}\right)^2 + \cdots} \tag{A.5}$$

The uncertainty calculated from (A.5) is used in (A.2) to estimate the uncertainty of the relative absorption refractive index function.

References

1. H. Zhao, N. Ladommatos, Prog. Energy Combust. Sci. **24**, 221 (1998)
2. H. Moosmüller, R.K. Chakrabarty, W.P. Arnott, J. Quant. Spectrosc. Radiat. Transf. **110**, 844 (2009)
3. F. Liu, K.A. Thomson, G.J. Smallwood, Appl. Phys. B, Lasers Opt. **96**, 671 (2009)
4. D.R. Snelling, K.A. Thomson, G.J. Smallwood, Ö.L. Gülder, E.J. Weckman, R.A. Fraser, AIAA J. **40**, 1789 (2002)
5. S. De Iuliis, M. Barbini, S. Benecchi, F. Cignoli, G. Zizak, Combust. Flame **115**, 253 (1998)
6. B.M. Crosland, M.R. Johnson, K.A. Thomson, Appl. Phys. B **102**(1), 173–183 (2011)
7. W.H. Dalzell, A.F. Sarofim, J. Heat Transf. **91**, 100 (1969)
8. B.J. Stagg, T.T. Charalampopoulos, Combust. Flame **94**, 381 (1993)
9. H. Chang, T.T. Charalampopoulos, Proc. R. Soc. Lond. Ser. A, Math. Phys. Sci. **430**, 577 (1990)
10. J. Mullins, A. Williams, Fuel **66**, 277 (1987)
11. M. Schnaiter, H. Horvath, O. Mohler, K.H. Naumann, H. Saathoff, O.W. Schock, J. Aerosol Sci. **34**, 1421 (2003)
12. S.S. Krishnan, K.C. Lin, G.M. Faeth, J. Heat Transf. **122**, 517 (2000)
13. S.C. Lee, C.L. Tien, Proc. Combust. Inst. **18**, 1159 (1981)
14. Ü.Ö. Köylü, G.M. Faeth, J. Heat Transf. **118**, 415 (1996)
15. C.W. Bruce, T.F. Stromberg, K.P. Gurton, J.B. Mozer, Appl. Opt. **30**, 1537 (1991)
16. D.R. Snelling, F. Liu, G.J. Smallwood, Ö.L. Gülder, Combust. Flame **136**, 180 (2004)
17. R.A. Dobbins, G.W. Mulholland, N.P. Bryner, Atmos. Environ. **28**, 889 (1994)
18. J.S. Wu, S.S. Krishnan, G.M. Faeth, J. Heat Transf. **119**, 230 (1997)
19. S. De Iuliis, F. Migliorini, F. Cignoli, G. Zizak, Appl. Phys. B **83**, 397 (2006)
20. R.A. Dobbins, C.M. Megaridis, Langmuir **3**, 254 (1987)
21. A.D. Abid, N. Heinz, E.D. Tolmachoff, D.J. Phares, C.S. Campbell, H. Wang, Combust. Flame **154**, 775 (2008)
22. H. Bladh, J. Johnsson, P.-E. Bengtsson, Appl. Phys. B **96**, 645 (2009)
23. G. Cléon, T. Amodeo, A. Faccinetto, P. Desgroux, Appl. Phys. B (2011, submitted)
24. B. Therssen, Y. Bouvier, C. Schoemaecker-Moreau, X. Mercier, P. Desgroux, M. Ziskind, C. Focsa, Appl. Phys. B **89**, 417 (2007)
25. F. Liu, D.R. Snelling, in *AIAA 40th Thermophysics Conference* (AIAA, Washington, 2008). Paper No. 2008-4362
26. H. Bladh, J. Johnsson, N.E. Olofsson, A. Bohlin, P.-E. Bengtsson, Proc. Combust. Inst. **33**(1), 641–648 (2011)
27. A. D'Anna, Proc. Combust. Inst. **32**, 593 (2009)
28. S.C. Graham, Proc. Combust. Inst. **16**, 663 (1976)
29. J. Zerbs, K.P. Geigle, O. Lammel, J. Hader, R. Stirn, R. Hadef, W. Meier, Appl. Phys. B **96**, 683 (2009)
30. J. Appel, B. Jungfleisch, M. Marquardt, R. Suntz, H. Bockhorn, Proc. Combust. Inst. **26**, 2387 (1996)
31. A. Lamprecht, W. Eimer, K. Kouse-Höinghaus, Combust. Flame **118**, 140 (1999)
32. D.R. Snelling, K.A. Thomson, G.J. Smallwood, Ö.L. Gulder, Appl. Opt. **38**, 2478 (1999)
33. B. Axelsson, R. Collin, P.-E. Bengtsson, Appl. Opt. **39**, 3683 (2000)
34. B. Axelsson, R. Collin, P.-E. Bengtsson, Appl. Phys. B **72**, 367 (2001)
35. C.P. Arana, M. Pontoni, S. Sen, I.K. Puri, Combust. Flame **138**, 362 (2004)
36. K. Lee, Y. Han, W. Lee, J. Chung, C. Lee, Meas. Sci. Technol. **16**, 519 (2005)
37. L.L. McCrain, W.L. Roberts, Combust. Flame **140**, 60 (2005)
38. M.D. Smooke, M.B. Long, B.C. Connelly, M.B. Colket, R.J. Hall, Combust. Flame **143**, 613 (2005)
39. B.F. Kock, B. Tribalet, C. Schulz, P. Roth, Combust. Flame **147**, 79 (2006)
40. J.V. Pastor, J.M. Garcia, J.M. Pastor, J.E. Buitrago, Meas. Sci. Technol. **17**, 3279 (2006)
41. A. Fuentes, G. Legros, H. El-Rabii, J.P. Vantelon, P. Joulain, J.L. Torero, Exp. Fluids **43**, 939 (2007)
42. A.V. Menon, S.-Y. Lee, M.J. Linevky, T.A. Litzinger, R.J. Santoro, Proc. Combust. Inst. **31**, 593 (2007)
43. S.S. Iyer, T.A. Litzinger, S.-Y. Lee, R. Santoro, Combust. Flame **149**, 206 (2007)
44. K.A. Thomson, M.R. Johnson, D.R. Snelling, G.J. Smallwood, Appl. Opt. **47**, 694 (2008)
45. A.E. Karatas, M. Commodo, Ö.L. Gulder, Energy Fuels **24**, 4912 (2010)
46. R.A. Dobbins, H. Subramaniasivam, in *Springer Ser. Chem. Phys.*, vol. 59 (1994), p. 290
47. R.J. Santoro, J.H. Miller, Langmuir **3**, 244 (1987)
48. D.W. Senser, J.S. Morse, V.A. Cundy, Rev. Sci. Instrum. **56**, 1279 (1985)
49. W. Clauss, V.I. Fabelinsky, D.N. Kozlov, V.V. Smirnov, O.M. Stelmakh, K.A. Vereschagin, Appl. Phys. B **70**, 127 (2000)
50. S. Cheskis, Prog. Energy Combust. Sci. **25**, 233 (1999)
51. R.S. Barlow, C.D. Carter, Combust. Flame **97**, 261 (1994)
52. W. Meier, A.O. Vyrodov, V. Bergmann, W. Stricker, Appl. Phys. B **63**, 79 (1996)
53. A. D'Alessio, G. Gambi, P. Minutolo, S. Russo, A. D'Anna, Proc. Combust. Inst. **25**, 645 (1994)
54. F. Xu, P.B. Sunderland, G.M. Faeth, Combust. Flame **108**, 471 (1997)
55. B. Atakan, A. Lamprecht, K. Kohse-Hoinghaus, Combust. Flame **133**, 431 (2003)
56. B. Apicella, M. Alfé, R. Barbella, A. Tregrossi, A. Ciajolo, Carbon **42**, 1583 (2004)
57. V. Kruger, C. Wahl, R. Hadef, K.P. Geigle, W. Stricker, M. Aigner, Meas. Sci. Technol. **16**, 1477 (2005)
58. C. Schulz, B.F. Kock, M. Hofmann, H. Michelsen, S. Will, B. Bougie, R. Suntz, G. Smallwood, Appl. Phys. B **83**, 333 (2006)
59. T.C. Bond, R.W. Bergstrom, Aerosol Sci. Technol. **40**, 1 (2006)
60. M.O. Andreae, A. Gelencser, Atmos. Chem. Phys. **6**, 3131 (2006)

61. A.I. Medalia, L.W. Richards, J. Colloid Interface Sci. **40**, 233 (1972)
62. M. Alfé, B. Apicella, R. Barbella, J.N. Rouzaud, A. Tregrossi, A. Ciajolo, Proc. Combust. Inst. **32**, 697 (2009)
63. T.C. Williams, C.R. Shaddix, K.A. Jensen, J.M. Suo Anttila, Int. J. Heat Mass Transf. **50**, 1616 (2007)
64. H.H. Grotheer, H. Pokorny, K.L. Barth, M. Thierley, M. Aigner, Chemosphere **57**, 1335 (2004)
65. A. D'Alessio, A. D'Anna, A. D'Orsl, P. Minutolo, R. Barbella, Proc. Combust. Inst. **24**, 973 (1992)
66. R.A. Dobbins, R.A. Fletcher, W. Lu, Combust. Flame **100**, 301 (1995)
67. S.S. Krishnan, K.C. Lin, J.S. Wu, G.M. Faeth, in *Proceedings of the 1997 ASME Winter Annual Meeting*, Dallas, TX, vol. 352 (1997), p. 39
68. Ü.Ö. Köylü, G.M. Faeth, J. Heat Transf. **115**, 409 (1993)
69. K.A. Thomson, M.R. Johnson, D.R. Snelling, G.J. Smallwood, Appl. Opt. **47**, 694 (2008)
70. P.S. Greenberg, J.C. Ku, Appl. Opt. **36**, 5514 (1997)
71. R.A. Dobbins, C.M. Megaridis, Appl. Opt. **30**, 4747 (1991)
72. Ü.Ö. Köylü, G.M. Faeth, Combust. Flame **89**, 140 (1992)
73. C.M. Sorensen, Aerosol Sci. Technol. **35**, 648 (2001)
74. A.R. Coderre, K.A. Thomson, D.R. Snelling, M.R. Johnson, Appl. Phys. B (2011, submitted)
75. Ö.L. Gülder, D.R. Snelling, R.A. Sawchuk, Proc. Combust. Inst. **28**, 2351 (1996)
76. A. Ciajolo, R. Ragucci, B. Apicella, R. Barbella, M. De Joannon, A. Tregrossi, Chemosphere **42**, 835 (2001)
77. A. Ciajolo, A. Tregrossi, R. Barbella, R. Ragucci, B. Apicella, M. De Joannon, Combust. Flame **125**, 1225 (2001)
78. T.L. Farias, M.G. Carvalho, U.O. Koylu, G.M. Faeth, J. Heat Transf. **117**, 152 (1995)
79. T.L. Farias, U.O. Koylu, M.G. Carvalho, Appl. Opt. **35**, 6560 (1996)
80. F. Liu, D.R. Snelling, in *AIAA 40th Thermophysics Conference* (AIAA, Washington, 2008). Paper No. 2008-4362